

AFM Characterization of Ta-based Diffusion Barriers for Use in Future Semiconductor Metallization

D. Fischer,^{1,*}† O. Meissner,² B. Bendjus,² J. Schreiber,² M. Stavrev¹ and C. Wenzel¹

¹ TU Dresden, Semiconductor and Microsystems Technology Laboratory, Dresden, Germany

² Fraunhofer Institute for Nondestructive Testing (IZFP), EADQ Dresden, Germany

In this paper the investigation of r.f.-sputter-deposited Ta, Ta-N and Ta-N-O thin films is presented. Using atomic force microscopy in combination with sheet resistance measurements, Auger electron spectroscopy and x-ray diffraction, the thin film properties and microstructure are examined. Two crystalline modifications of Ta (tetragonal β -Ta and bcc α -Ta) are reported. By incorporation of nitrogen and/or oxygen into the Ta films, nanocrystalline and quasi-amorphous structures can be achieved. Finally, the usefulness of the films as diffusion barriers in Cu-based metallization systems is described. © 1997 by John Wiley & Sons, Ltd.

Surf. Interface Anal. 25, 522-528 (1997)

No. of Figures: 7 No. of Tables: 2 No. of Refs: 12

KEYWORDS: Ta; diffusion barriers; nanocrystalline films; amorphous films; AFM

INTRODUCTION

The development of advanced metallization systems, consisting of contacts, vias, interconnects and interlevel dielectrics, plays a key role in the concept for future integrated circuits. Concerning the interconnects, there is a growing interest in using Cu instead of Al alloys due to better electromigration resistance and lower resistivity. But several problems must be overcome. One of the major concerns, the thermal stability of the metallization system, is essential for the device performance. It is well known that a stable barrier is necessary to avoid undesired diffusion and/or reaction between the Cu and the Si substrate or the interlevel dielectric. Many diffusion barriers for Cu metallization have been investigated.¹ Among these materials, Ta alloys are considered to be the most promising diffusion barriers,²⁻⁷ due to the high electrical conductivity, high chemical inertness and immiscibility between Cu and Ta. Unfortunately, most of these barriers are polycrystalline and provide inadequate protection because they contain grain boundaries serving as fast diffusion paths for Cu. Further improvement of the barrier stability can be achieved by alloying Ta with N and/or O, leading to a quasi-amorphous structure.⁷

Because the diffusion barrier has to become thinner, it is necessary to pay particular attention to the microstructure of the barrier. However, conventional methods for material characterization, e.g. optical and electron

microscopy, are becoming inappropriate due to either low resolution or low efficiency. Scanning probe microscopy (SPM) techniques, and especially atomic force microscopy (AFM),⁸ are emerging as powerful tools to gain insight into the microstructure of thin films on the nanometre scale. But, surprisingly, we could not find any basic research results for SPM characterization in the literature concerning the development of diffusion barriers. This work presents AFM microstructural investigations on thin sputter-deposited Ta and reactively sputtered Ta-N and Ta-N-O diffusion barriers.

EXPERIMENTAL

For the study of the Ta-based thin films, 4-in. blanket and oxidized $\langle 111 \rangle$ and $\langle 100 \rangle$ Si wafers were used. All cleaning and deposition steps were performed on a cluster tool consisting of load-lock, dealer, Ta physical vapour deposition (PVD) module and inductively coupled plasma (ICP) etch module for soft cleaning the surface. The nominal base pressure in the PVD chamber is specified to be 10^{-6} Pa. After soft-etch-cleaning and without breaking the vacuum, 5, 10, 20, 50 and 100 nm thin films were deposited. Process parameters for deposition of Ta, Ta-N and Ta-N-O barriers are summarized in Table 1.

The thickness of the Ta-based films down to 20 nm was analysed by surface profilometry using a TENCOR Alpha Step 500 profilometer. For the determination of the 5 and 10 nm film thicknesses, a calculated deposition rate was fitted in. Sheet resistivities were obtained by conventional four-point probe measurements. The film composition was determined by AES in combination with Ar sputter etching. For x-ray diffraction

* Correspondence to: D. Fischer, TU Dresden, Semiconductor and Microsystems Technology Laboratory, Dresden, Germany.

† Present address: TU Dresden, Institut für Halbleiter und Mikrosystemtechnik, 01062 Dresden, Germany

Contract grant sponsor: VW-Stiftung.

Table 1. Summary of parameters for tantalum thin film deposition

Parameter	Ta	Ta-N	Ta-N-O
P_{target}	500–1000 W	1000 W	1000 W
$T_{\text{substrate}}$	RT–600 °C	RT	RT
Ar flow	5 sccm	5 sccm	5 sccm
N_2 flow	–	0–5 sccm	0–5 sccm
O_2 flow	–	–	0–10 sccm
Sputtering time (100 nm film)	2.5–5 min	2–10 min	2–20 min

(XRD) analysis, a thin film attachment equipped with a Cu $K\alpha$ source at a glancing angle of 2° was used.

The AFM measurements were performed with a Nanoscope III, (Dimension 3000, Digital Instruments) in contact mode using silicon tips. By using this equipment the acquisition of both topography and friction data is possible. Root mean square (RMS) roughness values were obtained using Nanoscope software and the mean grain size was calculated by measurement of 10 line scans across 250 × 250, 500 × 500 and 1000 × 1000 nm² areas.

RESULTS

Conventional characterization

The experimental set-up was chosen to deposit thin films as effective diffusion barriers.⁹ Figure 1 shows the dependence of the deposition rate and resistivity of Ta-based films on the nitrogen and oxygen flow rates, which could be clearly distinguished between a high-rate metal-sputtering mode (without or with low nitrogen and oxygen flow rate) and a low-rate compound-sputtering mode (at high nitrogen and oxygen flow rate). Concurrently, the film resistivity correlates with the deposition rate and thus high deposition rate results in low-resistivity films, and vice versa. In view of the demands on diffusion barriers, we have concentrated the investigations on the low-resistivity films.⁹

Table 2 summarizes the results regarding film composition and structural analysis obtained by AES and XRD measurements. Pure Ta films deposited at substrate temperatures lower than 400 °C grow in the tetragonal modification (β -Ta; Fig. 2). On the other

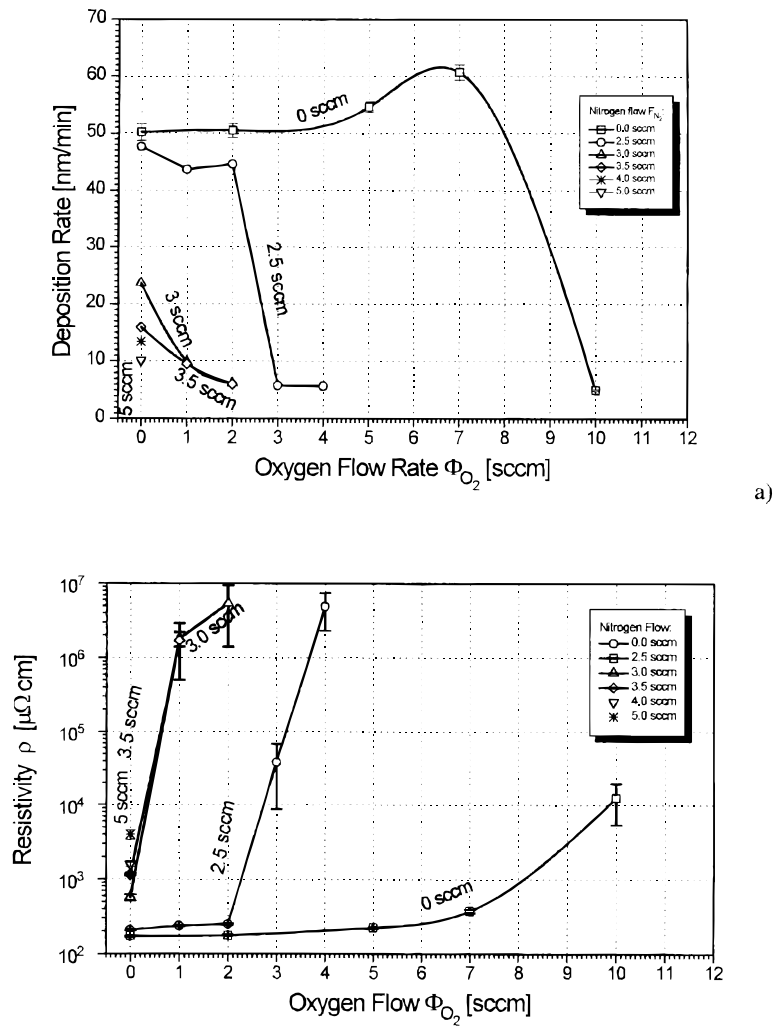


Figure 1. Dependence of deposition rate and resistivity of Ta-N-O films on the composition of sputtering gas mixture.

Table 2. Selected properties of some Ta-based thin films

Thin film	Process parameters	Structure	Film composition (%)
Ta	$P_{\text{target}} = 500 \text{ W}$ $T_{\text{substrate}} > 400 \text{ }^\circ\text{C}$ Ar flow = 5 sccm	bcc (α -Ta)	Ta = 100
	$P_{\text{target}} = 500 \text{ W}$ $T_{\text{substrate}} \leq 400 \text{ }^\circ\text{C}$	tetragonal (β -Ta)	Ta = 100
Ta-N	$P_{\text{target}} = 1000 \text{ W}$ $T_{\text{substrate}} = \text{RT}$ Ar flow = 5 sccm		
	N_2 flow < 2.5 sccm	tetr. Ta + bcc Ta(N)	–
	N_2 flow = 2.5 sccm N_2 flow = 3.5 sccm	bcc Ta(N) fcc TaN	Ta/N = 77:23 Ta/N = 48:52
Ta-N-O	$P_{\text{target}} = 1000 \text{ W}$ $T_{\text{substrate}} = \text{RT}$ Ar flow = 5 sccm N_2 flow = 2.5 sccm O_2 flow = 2.0 sccm	bcc Ta(N, O)	Ta/N/O = 81:16:3

hand, increasing the substrate temperature leads to bcc Ta films (α -Ta). At room temperature, the addition of N_2 to the sputtering gas results in the continuous transformation from tetragonal to a bcc phase with pure bcc Ta(N) at 2.5 sccm N_2 flow (see Fig. 2). Further addition of O_2 up to 2 sccm preserves the bcc modification. Furthermore, peak broadening and shift to lower 2θ angles become obvious with increasing reactive gas flows. For these described Ta(N, O) films, nitrogen and oxygen contents of ~ 16 at.% and ~ 3 at.%, respectively, were estimated by AES.

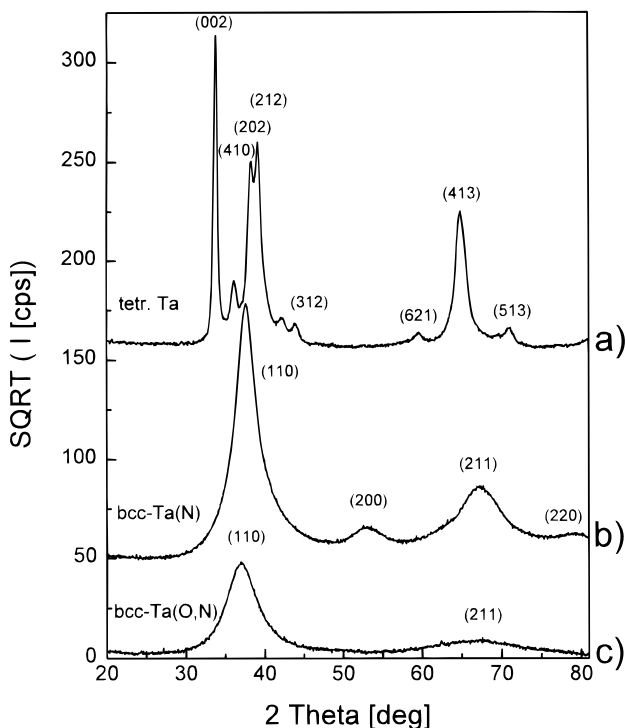
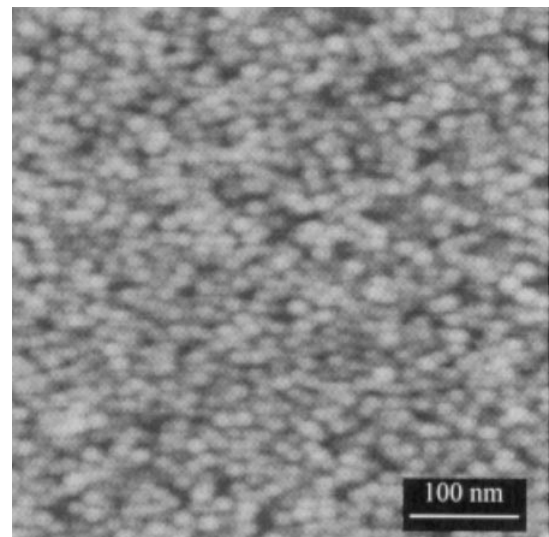
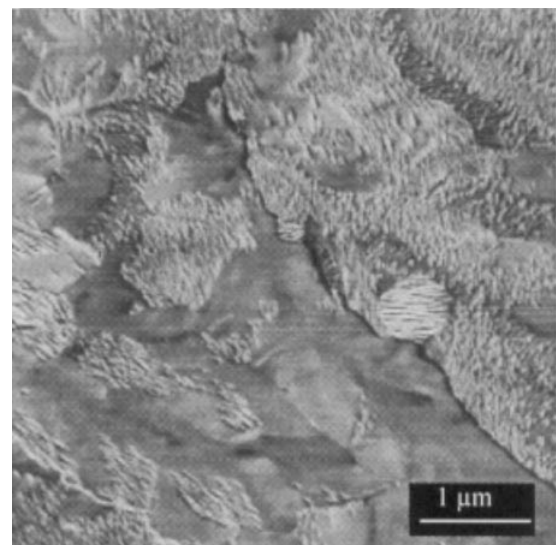


Figure 2. X-ray diffraction patterns of Ta-based films; (a) $P_T = 1$ kW; Ar = 5 sccm; (b) $P_T = 1$ kW; Ar = 5 sccm; $N_2 = 2.5$ sccm; (c) $P_T = 1$ kW; Ar = 5 sccm; $N_2 = 2.5$ sccm; $O_2 = 2$ sccm.



(a)



(b)

Figure 3. The AFM images of 100 nm Ta films; (a) β -Ta; $T_{\text{substrate}} = 25 \text{ }^\circ\text{C}$; (b) α -Ta; $T_{\text{substrate}} = 450 \text{ }^\circ\text{C}$.

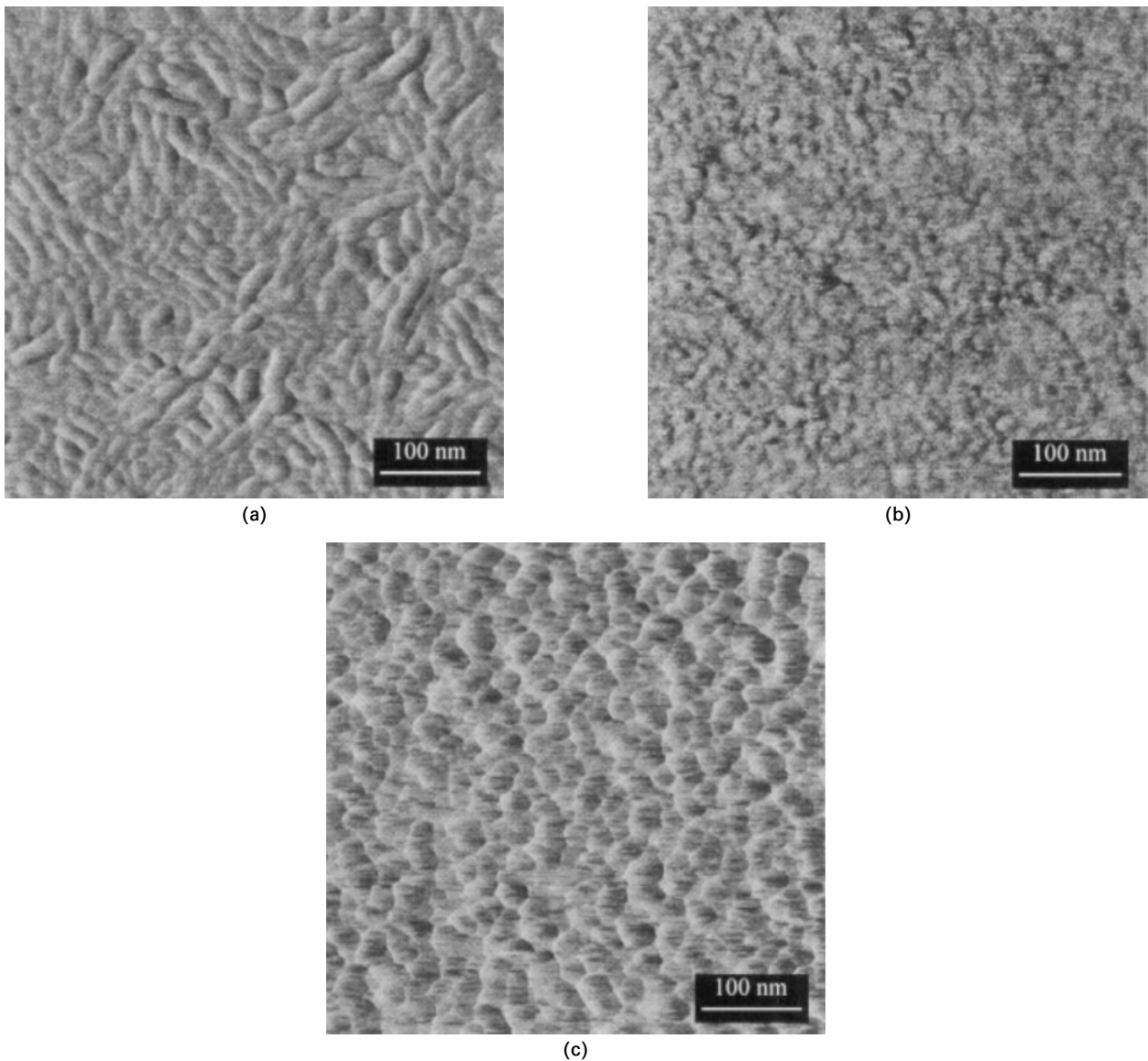


Figure 4. The AFM images of 100 nm Ta-N films: (a) bcc Ta(N): 1.5 sccm N_2 , RMS \sim 0.7 nm; (b) bcc Ta(N): 2.5 sccm N_2 , RMS \sim 0.25 nm; (c) fcc TaN: 3.5 sccm N_2 , RMS \sim 1.8 nm.

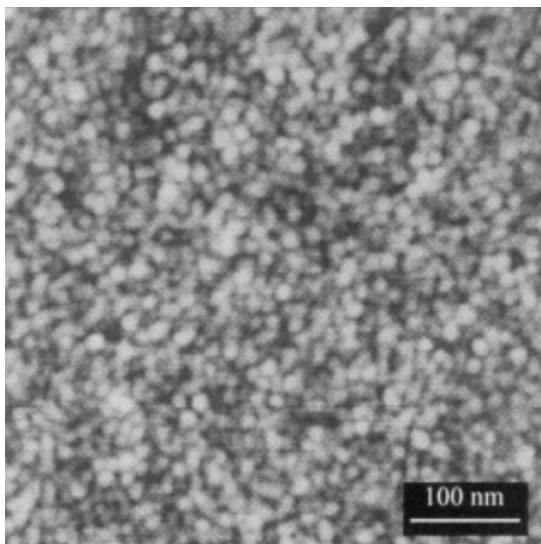


Figure 5. The AFM image of a 100 nm bcc Ta(N, O) film. Parameters: power = 1 kW; argon = 5 sccm; N_2 = 2.5 sccm; O_2 = 2 sccm.

Increasing the N_2 flow above 2.5 sccm leads to the formation of several Ta-N phases, i.e. fcc TaN at 3.5 sccm N_2 , associated with enlarged incorporation of nitrogen into the film.

As impurities, small amounts of argon, carbon and oxygen were detected in all films.

Atomic force microscopy characterization

The comparison between 100 nm low-temperature β -Ta and high-temperature α -Ta films is presented in Fig. 3. The AFM measurements for the β -Ta film show circular grains of 15 nm in diameter. On the other hand, the α -Ta films consist of large unequal regions of several square microns in area. Additionally, small lamellar-shaped substructures are observed.

The dependence of the film microstructure on the nitrogen gas flow is plotted in Fig. 4. The addition of 1.5 sccm N_2 predominantly results in randomly distrib-

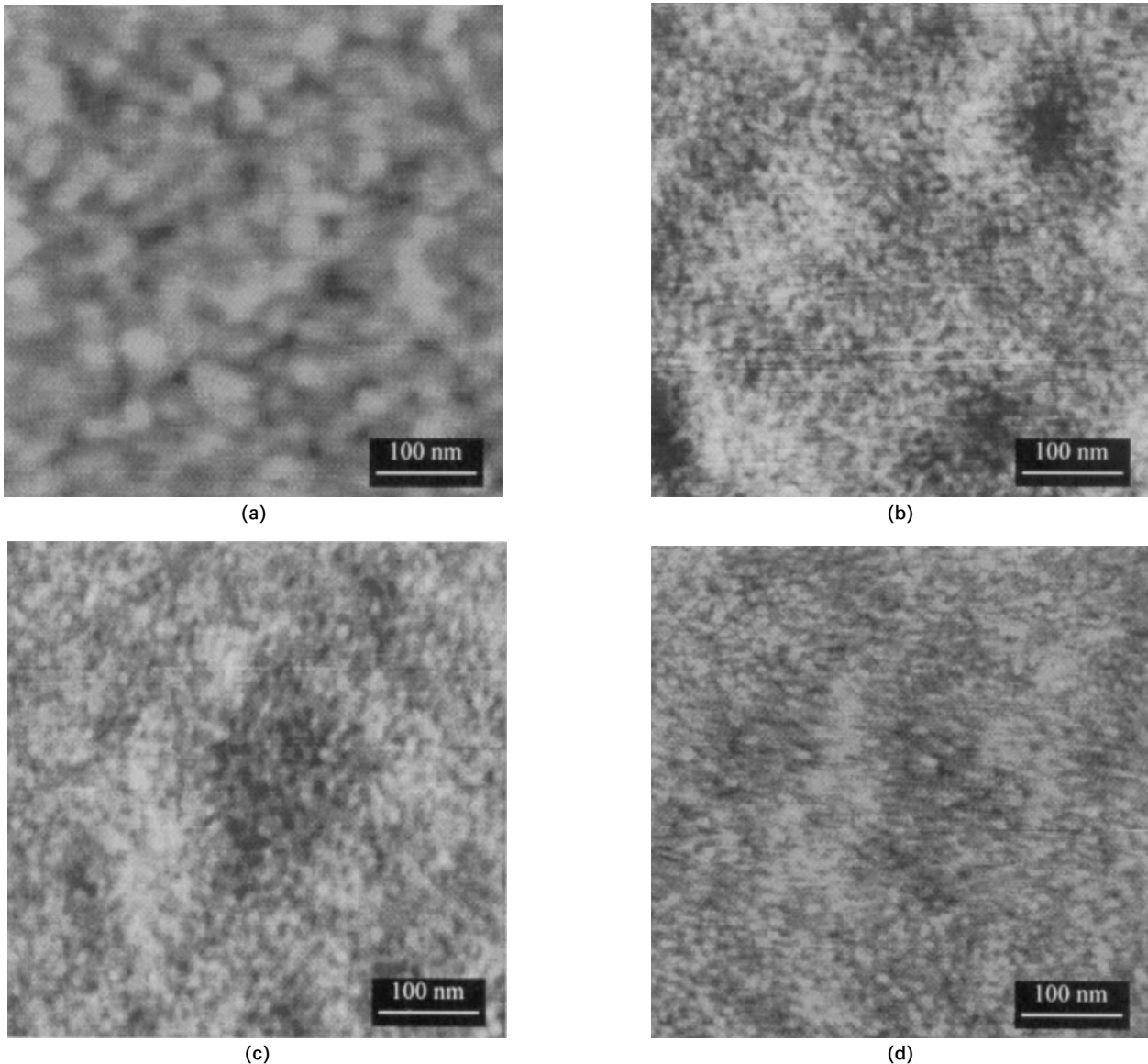


Figure 6. The AFM image of: (a) 500 nm SiO_2 surface without film coating; (b) 5 nm $\beta\text{-Ta}$: Ar = 5 sccm; (c) 5 nm bcc Ta(N): Ar = 5 sccm, N_2 = 2.5 sccm; (d) 5 nm bcc Ta(N, O): Ar = 5 sccm, N_2 = 2.5 sccm, O_2 = 2 sccm.

uted elongated grains 10–20 nm wide and 80 nm long. The AFM image at 2.5 sccm N_2 [Fig. 4(b)] shows a very smooth surface (RMS \sim 0.25 nm). No distinct structure could be detected. In contrast, the films sput-

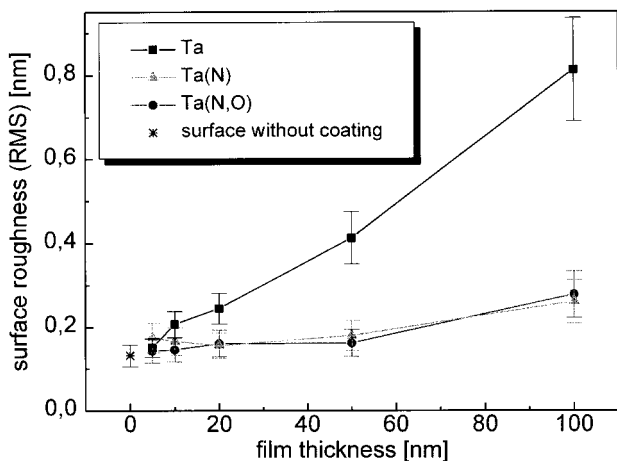


Figure 7. Dependence of the surface roughness on the film thickness for $\beta\text{-Ta}$, bcc Ta(N) and bcc Ta(N, O) films.

tered at 3.5 sccm N_2 exhibit higher surface roughness (RMS \sim 1.8 nm) and a clear polycrystalline structure with a mean grain size of \sim 25 nm.

As shown in Fig. 5, the addition of 2 sccm O_2 to the gas mixture of 5 sccm Ar and 2.5 sccm N_2 for the deposition of 100 nm Ta(N, O) leads to nearly the same microstructure and surface roughness (RMS \sim 0.28 nm) as compared to the Ta(N) film sputtered at 2.5 sccm N_2 .

To investigate the film thickness effect on the microstructure, AFM measurements were carried out on 5, 10, 20, 50 and 100 nm Ta-based films. A set of AFM images showing the surface of an uncoated sample and of various 5 nm thin films is plotted in Fig. 6. The image of the sample without coating shows an initial roughness of 0.13 nm. Covering these samples with 5 nm Ta, Ta(N) or Ta(N, O) leads to a slight increase in surface roughness between 0.15 and 0.18 nm. Concurrently, the maximum height difference over the whole scan area is measured to be $<$ 2 nm. This means that with the nominal thickness of 5 nm, a complete coverage of the surface was obtained. Figure 7 gives the relationship between RMS surface roughness and film thickness for

β -Ta, Ta(N) and Ta(N, O). While the RMS values for Ta(N) and Ta(N, O) are nearly independent of the film thickness, the roughness for β -Ta increases with increasing film thickness.

DISCUSSION

Thin films of Ta

Using r.f. magnetron sputtering it is possible to deposit two kinds of Ta film. The high-temperature α -Ta films grow in a crystalline state with grain sizes of several microns. The grain boundaries and substructures revealed by AFM could be considered as extended defects acting as fast diffusion paths. This feature could considerably restrict the efficiency, especially of very thin barriers.

According to the AFM measurements, the low-temperature modification seems to be crystalline with small grains. Except for the observed grain boundaries, we could not find any larger defects. Images like those of β -Ta [Fig. 3(a)] are typical for columnar-grown grains, where the boundaries could work as channels for Cu diffusion. Another argument for probable columnar growth is the thickness dependence of the film roughness (Fig. 7), which could be explained by self-shadowing during deposition.¹⁰ Because the conventional AFM technique is not able to provide subsurface information at different depths, reliable predictions on barrier performance are not possible.

Thin films of Ta-N

As described already, addition of N₂ up to 2.5 sccm gas flow results in a phase transformation from tetragonal to bcc phase. As can be concluded from the peak shift in the corresponding XRD pattern as compared to the bcc-Ta phase (JCPDS-ICDD 4-788), the nitrogen atoms are completely incorporated into the Ta lattice. The peak width suggests a very small grain size, which is in good agreement with the corresponding AFM images [Figs 4(b) and 6(c)]. The roughness of these films is nearly independent of the film thickness (see Fig. 7). This is further confirmation for the non-columnar nanocrystalline structure, which is quite favourable for barriers.

Films with higher nitrogen content crystallize more strongly, as shown with the fcc TaN film deposited at 3.5 sccm N₂ flow. The AFM images [Fig. 4(c)] are comparable to those of the tetragonal Ta. The only difference is that the grain size of the fcc TaN films is slightly larger than that of β -Ta.

Thin films of Ta-N-O

Films reactively deposited in a gas mixture of Ar-N₂-O₂ (5:2.5:2) show XRD patterns (Fig. 2) with only two very broad peaks comparable to the (110) and (211) peaks of the bcc Ta(N) phase. The further shift in peak position towards smaller 2 θ angles reveals a

further increase of spacing of the lattice, which is due to interstitial oxygen incorporation into the bcc lattice. The decreasing number and the shape of the peaks indicate the growth of a quasi-amorphous structure. The AFM image (Fig. 5) does not show significant differences as compared to the image from the bcc Ta(N). But the roughness of the Ta(N, O) films below 20 nm film thickness is slightly smaller as compared to that of the Ta(N) films, probably due to the higher degree of amorphization.

CONCLUSION

This work presents investigations on sputter-deposited Ta-based thin films. Using the AFM technique in combination with conventional methods for material analysis, it was possible to examine the film microstructure on a nanometre scale. The major results can be summarized as follows:

- (1) α -Ta films deposited above 400 °C substrate temperature are crystalline with grain sizes in the micro-metre range and distinct grain boundaries,
- (2) β -Ta films deposited below 400 °C substrate temperature are apparently crystalline with grain sizes of ~15 nm, depending on the film thickness,
- (3) the addition of nitrogen up to 2.5 sccm N₂ results in nanocrystalline bcc Ta(N) films with reduced roughness and smaller grain sizes as compared to β -Ta films. The further addition of oxygen leads to quasi-amorphous bcc Ta(N, O) films.

Due to the observed grain boundaries, the performance of both α - and β -Ta films could be limited to applications where either thicker (≥ 100 nm) diffusion barriers are possible or moderate temperatures have to be sustained.

The reactive sputtered films can be considered as very effective barriers against Cu diffusion, due to the lack of extended film defects and grain boundaries acting as short-circuit diffusion paths. Additionally, the Ta(N, O) films exhibit an extremely low roughness and so they are suitable as extremely thin diffusion barriers with high thermal stability.

By applying the conventional AFM technique, only the surface of the thin films could be characterized. But the development of future barriers requires the use of sophisticated characterization techniques that guarantee statements with a high degree of certainty regarding barrier performance. In particular, the acquisition of subsurface information seems to be necessary. This can be obtained, for example, by detection of ultrasonic vibration amplitude.¹¹ Subsurface properties could also be examined by investigation of the elastic compliance using force volume capabilities. The influence of topography is eliminated by subtraction of images made by the measurement of various forces.

Acknowledgements

Financial support for this work was provided by VW-Stiftung. The authors thank Dr N. Mattern for the XRD measurements, Dr A. John for the AES analysis and E. Fischer for the electrical measurements.

REFERENCES

1. S.-Q. Wang, *MRS Bull.* **XIX**(8), 30 (1994).
2. P. J. Pokela, C.-K. Kwok, E. Kolawa, S. Raud and M.-A. Nicolet, *Appl. Surf. Sci.* **53**, 364 (1991).
3. J. S. Reid, E. Kolawa, R. P. Ruiz and M.-A. Nicolet, *Thin Solid Films*, **236**, 319 (1993).
4. L. A. Clevenger, N. A. Bojarczuk, K. Holloway, J. M. E. Harper, C. Cabral, Jr., R. G. Schad, F. Cardone and L. Stolt, *J. Appl. Phys.* **73**(1) 300 (1993).
5. M. Stavrev, C. Wenzel, A. Möller and K. Drescher, *Appl. Surf. Sci.* **91**, 257 (1995).
6. C. Wenzel, M., Stavrev, F. Rudolf, A. Preuß, A. Möller and K. Drescher, in *Advanced Metallization for Integrated Systems and ULSI Applications*, pp. 291–297. MRS, Pittsburgh (1996).
7. M. Stavrev, D. Fischer, A. Preuß, C. Wenzel and N. Mattern, to be published in *Microelectron. Eng.*
8. G. Binnig, C. F. Quate and C. Gerber, *Phys. Rev. Lett.* **56**, 930 (1986).
9. H. P. Kattelus and M.-A. Nicolet, in *Diffusion Phenomena in Thin Films and Microelectronic Materials*, edited by D. Gupta and P. S. Ho, pp. 432–498. Noyes, Park Ridge, NJ (1988).
10. J. A. Thornton, *J. Vac. Sci. Technol.* **12**, 830 (1975).
11. U. Rabe and W. Arnold, *Appl. Phys. Lett.* **64**(12), 1493 (1994).
12. U. Rabe, K. Janser and W. Arnold, *Rev. Sci. Instrum.* **67**(9), 3281 (1996).